Front. Chem. Sci. Eng. 2021, 15(4): 1008–1020
https://doi.org/10.1007/s11705-020-1996-8

RESEARCH ARTICLE

Trihydrazinotriazine-grafting Fe_3O_4/SiO_2 core-shell nanoparticles with expanded porous structure for organic reactions

Jamal Rahimi*, Seyedeh Shadi Mirmohammadi*, Ali Maleki (✉)

Catalysts and Organic Synthesis Research Laboratory, Department of Chemistry, Iran University of Science and Technology, Tehran 16846-13114, Iran

Abstract This study focuses on the synthesis and characterization of a novel magnetic nanocomposite 2,4,6-trihydrazino-1,3,5-triazine (THDT)-functionalized with silica-coated iron oxide magnetic nanoparticles (MNPs). This nanocomposite has porous morphology decorated with the spherical MNPs. Through co-precipitation of iron salts, MNPs were obtained. The prepared THDT was placed on the chlorine surface-modified MNPs. The present environment-friendly nanocatalyst intensely accelerated the synthesis of highly functionalized tetrahydrobenzo[*b*]pyran derivatives as well as reduced the reaction times and increased yields of the products.

Keywords trihydrazino-triazine, porous, magnetic nanocatalyst, green chemistry, tetrahydrobenzo[*b*]pyrans

1 Introduction

There are several routes for the synthesis of magnetic nanoparticles (MNPs). Among them, the co-precipitation, hydrothermal reaction, and sol-gel methods, as well as microemulsion technique and microwave irradiation are widely used. Preservation of the optimized condition plays a prominent role in synthesizing MNPs in metals, alloys, iron oxide and ferrites. These MNPs are either great catalysts or can be substantial supporters for modification or functionalization of other catalysts. Fe_3O_4 MNPs are an excellent catalysis supporter due to their low cost and simple preparation. Because of their active surface, Fe_3O_4 MNPs can easily be immobilized or adsorb catalyst fragments, including metallic catalysts, organocatalyst, and enzymes. This feature makes Fe_3O_4 a remarkably sustainable catalyst [1–4].

Recently, the interaction between organic and inorganic materials has attracted much attention. Mixing homogeneous and heterogeneous substances and cross-linking of inorganic and organic materials is helping the master production of the commercial composite. Immobilization of organic functional groups like amine groups can be easily improved by coating Fe_3O_4 with silica. Moreover, surface coating with amine groups improves catalytic activity. A significant advantage of silica is making a natural attachment to organic compounds. This results in an organic-inorganic composite that can generate unique properties at the interface, and the reaction between them is of significant importance [5,6].

The substances with porous structure are distinctive among their counterparts. They have characteristic features such as low thermal mass, high surface area, and low density. Moreover, various processing routes can modify the type or intensity of these characteristics. Various macrostructures with diverse opened and closed porosity, pore size distribution and pore morphology have been created for a range of applications [7,8].

Nanoparticles are of great scientific interest as they are effectively a bridge between bulk materials and atomic or molecular structures. The properties of materials change as their size approaches the nanoscale and as the percentage of atoms at the surface of a material becomes significant. This is the most important reason for the emergence of catalytic properties in nanoparticles. By controlling the shape, size, and surface composition of nanoparticles, newer properties of catalysis can be created. Due to their catalysis performance, researchers use nanoparticles in a variety of important reactions in order to accelerate reactions. Magnetite nanoparticles are inexpensive and efficient catalysts used in a variety of reactions such as the

Received May 30, 2020; accepted July 25, 2020

E-mail: maleki@iust.ac.ir

*These authors contributed equally to this work.

oxidation/reduction and acid/base reactions. For instance, reduction of 4-nitrotoluene can be expedited using magnetite nanoparticles. They can also be used for CO oxidation. By mixing iron oxide and other materials, such as titanium, their application can be expanded [9,10].

The as-synthesized product tetrahydrobenzo[*b*]pyrans, which is surrounded by many heterocycles that contain medicinal properties, is widely utilized in a variety of biological applications. Due to their significant biological and pharmacological properties, recently unique procedures for the synthesis of the 2-aminochromenyl ring via multicomponent reaction have been developed. On the account of their extended potential in biological, pharmacological, and environmental applications, the synthesis, surface modification, and characterization of MNPs have attracted much attention [11].

In this paper, building on previous studies [12–16], we propose a novel superparamagnetic heterogeneous catalyst through organic synthesis, and as for the application, the prepared catalyst Fe_3O_4@SiO_2-THDT was efficiently used in one-pot synthesis of tetrahydrobenzo[*b*]pyrans **4a**–**4p** via the condensation of aldehydes **1**, diketone **2** and malononitrile **3** (Scheme 1). To the best of the authors' knowledge, the design, preparation and characterization of Fe_3O_4@SiO_2-THDT nanocomposite have never been studied. In addition to their application in organic synthesis of tetrahydrobenzo[*b*]pyrans this novel, eco-friendly, efficient catalyst can be used in a vast number of chemical reactions. Furthermore, due to using ethanol, our proposed process can be used in green chemistry.

2 Experimental

2.1 General

Chemicals and reagents were purchased from Aldrich-Merck, Merck. The melting points of the samples were measured on an Electrothermal 9100 apparatus and were uncorrected. The Fourier transform infrared (FTIR) spectra were recorded using a Shimadzu IR-470 spectrometer by the method of KBr pellet, and scanning electron microscopy (SEM) images were captured using a Sigma VP-ZEISS microscope with an attached camera. Vibrating-sample magnetometer (VSM) magnetic measurements of the solid samples were recorded using Lakeshore 7407. The X-ray diffraction (XRD) patterns of the nanocatalyst powders were recorded with an X' pert Pro X-ray diffractometer operating at 40 mA, 40 kV. A Numerix DXP-X10P recorded energy dispersive X-ray (EDX) elemental analysis of the nanocatalyst, and thermal analysis was performed using a Bahr-STA 504 instrument under nitrogen atmosphere. ^{1}H nuclear magnetic resonance (^{1}H NMR, 500 and 400 MHz) spectra were obtained using Bruker Avance DRX-500 and 400, at ambient temperature, using TMS as internal standard and DMSO-d_6 as solvent.

2.2 Preparation of THDT

First, 1 g of cyanuric chloride was dissolved in 50 mL of dioxane and 1 mL of hydrazine hydrate 80% was dissolved in 25 mL of dioxane. Then the mixture of hydrazine hydrate and dioxane in a separator funnel was added dropwise to the combination of cyanuric chloride and dioxane. The mixture was stirred for an hour and was refluxed for 5 h at 80 °C. When the resulting white powder cooled to room temperature, it was washed with dioxane and water till pH = 7 and then dried at room temperature in 85% yield [17].

2.3 Preparation of Fe_3O_4 nanoparticles

Using the co-precipitation method, the Fe_3O_4 superparamagnetic nanoparticles were synthesized. The synthetic route uses $FeCl_2 \cdot 4H_2O$ and $FeCl_3 \cdot 6H_2O$ at a molar ratio of 1:2.5 in the presence of ammonia. Firstly, 2.5 g of $FeCl_3 \cdot 6H_2O$ and 1 g of $FeCl_2 \cdot 4H_2O$ were added in 70 mL of distilled water. While the temperature is reaching 60 °C, 20 mL ammonia was added dropwise to the combination. After stirring for 40 min, the mixture was cooled down to room temperature. The obtained black precipitate collected by an external magnet was intensely washed with ethanol and water [18].

2.4 Preparation of Fe_3O_4@SiO_2 nanocomposite

At first, 50 mg of Fe_3O_4 nanoparticles were dispersed in 20 mL of deionized water, and then 2.5 mL of ammonium hydroxide (25 wt-%) and 75 mL of ethanol were added to the Fe_3O_4 nanoparticles solution. Subsequently, 0.8 mL of tetraethyl orthosilicate was added dropwise to the mixture while stirring. Then it was stirred vigorously for 16 h at room temperature. The products were separated using an external magnet and were washed five times with ethanol and distilled water.

2.5 Preparation of Fe_3O_4@SiO_2-Cl nanoparticles

At first, 0.3 g of the obtained Fe_3O_4@SiO_2 nanocore-shell was added in 14 mL of tetrahydrofuran. In the sonication bath, 0.25 g of sodium hydride was dispersed in the mixture. After that, drop by drop, 2.2 mL of 3-chloropropyltriethoxysilane was mixed and then stirred vigorously for another 15 h at 65 °C. The obtained product was separated by an external magnet and washed with deionized water and ethanol. The precipitation was dried at 65 °C for 3 h.

2.6 Preparation of Fe_3O_4@SiO_2-THDT nanocatalyst

At first, 0.25 g of Fe_3O_4@SiO_2@3-chloropropyltriethoxysilane (Fe_3O_4@SiO_2-Cl) was dispersed in 25 mL of EtOH. Then, 0.25 mmol (27 mg) of 2,4,6-trihydrazino-

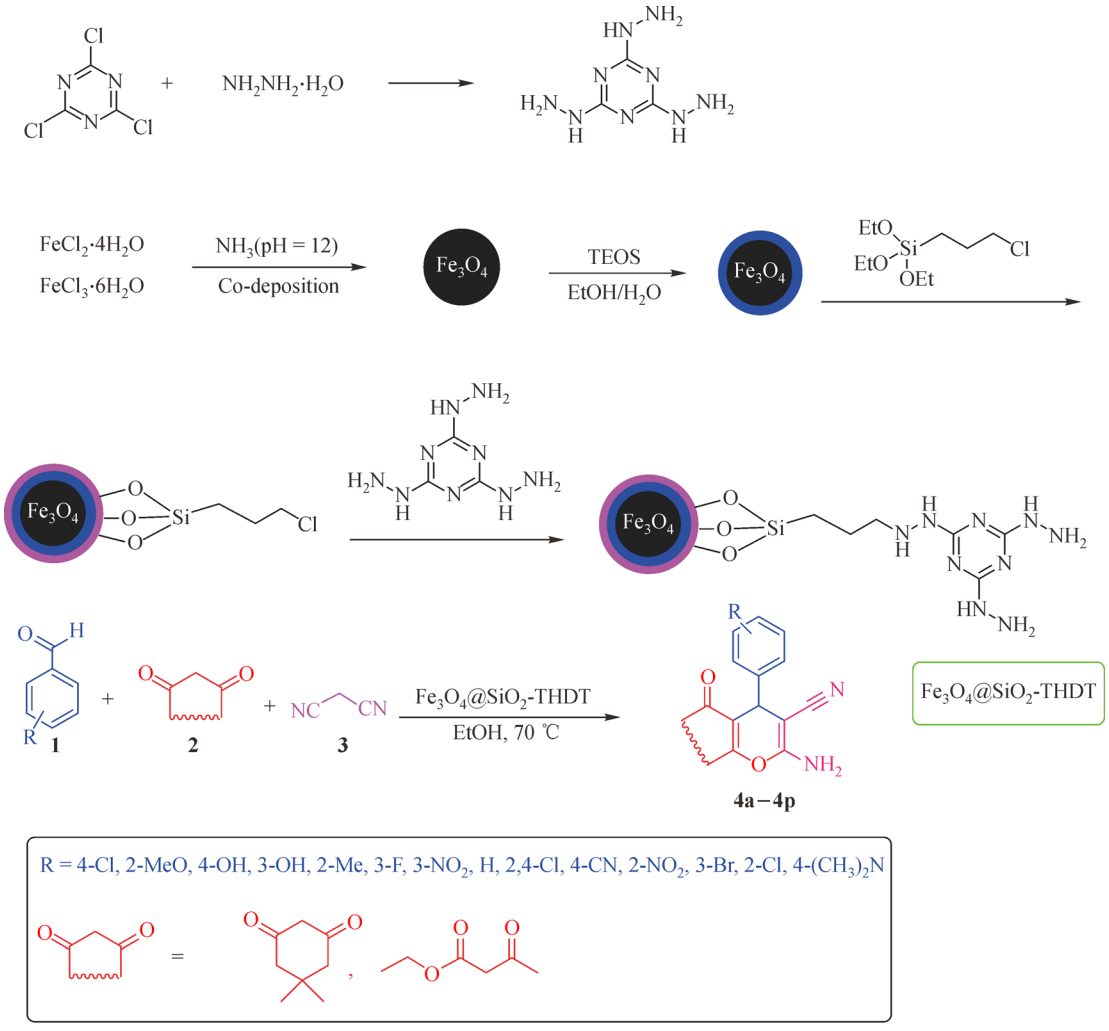

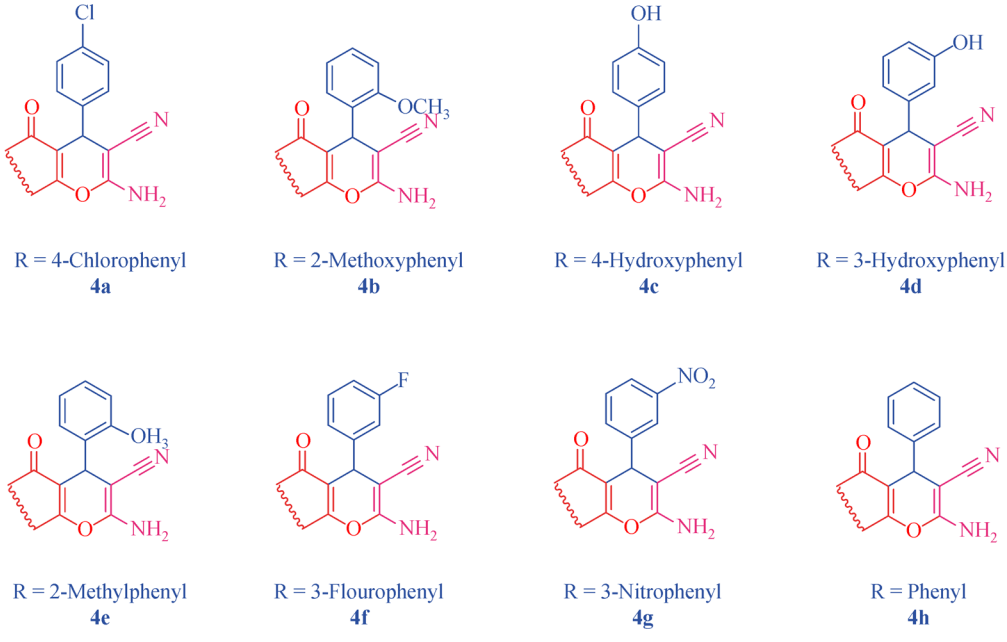

R = 4-Chlorophenyl **4a**

R = 2-Methoxyphenyl **4b**

R = 4-Hydroxyphenyl **4c**

R = 3-Hydroxyphenyl **4d**

R = 2-Methylphenyl **4e**

R = 3-Flourophenyl **4f**

R = 3-Nitrophenyl **4g**

R = Phenyl **4h**

Scheme 1 Fe_3O_4@SiO_2-THDT catalyst used in the synthesis of tetrahydrobenzo[*b*]pyrans **4a**–**4p**.

1,3,5-triazine was added and refluxed for 10 h. The resulting product was washed with EtOH and deionized water in sequence and dried at 65 °C for 10 h.

2.7 The synthesis of tetrahydrobenzo[*b*]pyrans derivatives **4a**–**4p**

Initially, 0.04 g of Fe_3O_4@SiO_2-THDT was added to a solution containing an aromatic aldehyde (1 mmol), *β*-ketoester (1 mmol), and Malononitrile (1.0 mmol) dissolved in ethanol. Then for 30 min, it was stirred at 75 °C it was stirred. The reaction progress was controlled by thin-layer chromatography (TLC). When the reaction finished, completion was confirmed by TLC, and cooled to room temperature, the catalyst was separated effortlessly by a magnet. Afterward, the crude product was isolated by filtration. Recrystallization from ethanol gave a more purified and crystalline product with 95% yield.

2.8 Spectra data of the selected products

2-Amino-3-cyano-4-(4-chlorophenyl)-7,7-dimethyl-5-oxo-4H-5,6,7,8-tetrahydrobenzo[b]pyran (**4a**). ^{1}H NMR (400 MHz, DMSO-d_6): δ 0.92 (s, 3H), 1.06 (s, 3H), 2.17 (d, J = 16.0 Hz, 2H), 2.19 (d, J = 16.0 Hz, 2H), 2.61 (s, 2H), 4.29 (s, 1H), 7.12 (s, 2H), 7.19 (2d, J = 8.2 Hz, 4H), 7.41 (2d, J = 8.2 Hz, 4H).

2-Amino-3-cyano-4-(2-methoxyphenyl)-7,7-dimethyl-5-oxo-4H-5,6,7,8-tetrahydrobenzo[b]pyran (**4b**). ^{1}H NMR (400 MHz, DMSO-d_6): δ 0.93 (s, 3H), 1.07 (s, 3H), 2.15–2.27 (m, 2H), 2.39 (s, 2H), 3.93 (s, 3H), 4.76 (s, 1H), 6.85 (brs, 2H), 7.31–7.74 (m, 4H).

2-Amino-3-cyano-4-(4-hydroxyphenyl)-5-oxo-4H-5,6,7,8-tetrahydrobenzo[b]pyran (**4c**). ^{1}H NMR (400 MHz, DMSO-d_6): δ 1.07 (s, 3H), 1.09 (s, 3H), 2.89 (s, 2H), 2.78 (m, 2H), 5.32 (s, 1H), 5.54 (s, 2H), 7.65–7.87 (m, 4H), 8.9 (s, 1H).

2-Amino-3-cyano-4-(3-hydroxyphenyl)-7,7-dimethyl-5-oxo-4H-5,6,7,8-tetrahydrobenzo[b]pyran (**4d**). ^{1}H NMR (400 MHz, DMSO-d_6): δ 0.97 (s, 3H), 1.04 (s, 3H), 2.09–2.28 (m, 2H), 2.45–2.56 (m, 2H), 4.07 (s, 1H), 6.54 (s, 2H), 6.58 (m, 1H), 6.97 (s, 1H), 7.04–7.08 (m, 1H), 9.32 (s, 1H).

2-Amino-3-cyano-4-(2-methylphenyl)-7,7-dimethyl-5-oxo-4H-5,6,7,8-tetrahydrobenzo[b]pyran (**4e**). ^{1}H NMR (400 MHz, DMSO-d_6): δ 0.94 (s, 3H), 1.07 (s, 3H), 2.10 (d, 1H), 2.23 (d, 1H), 2.36–2.58 (m, 2H), 2.75 (s, 3H), 4.39 (s, 1H), 6.03 (brs, 2H), 7.31–7.53 (m, 4H).

2-Amino-3-cyano-4-(3-fluorophenyl)-7,7-dimethyl-5-oxo-4H-5,6,7,8-tetrahydrobenzo[b]pyran (**4f**). ^{1}H NMR (500 MHz, DMSO-d_6): δ 0.95 (s, 3H), 1.02 (s, 3H), 2.11 (d, J = 16 Hz, 1H), 2.22 (d, J = 16 Hz, 1H), 2.47–2.55 (m, 2H), 4.22 (s, 1H), 6.91–7.34 (m, 6H).

2-Amino-3-cyano-4-(3-nitrophenyl)-7,7-dimethyl-5-oxo-4H-5,6,7,8-tetrahydrobenzo[b]pyran (**4g**). ^{1}H NMR (400 MHz, DMSO-d_6): δ 0.96 (s, 3H), 1.05 (s, 3H), 2.14–2.27 (m, 4H), 4.42 (s, 1H), 7.18 (s, 2H), 7.66 (s, 1H), 7.98–8.09 (m, 3H).

2-Amino-3-cyano-4-(phenyl)-7,7-dimethyl-5-oxo-4H-5,6,7,8-tetrahydrobenzo[b]pyran (**4h**). ^{1}H NMR (400 MHz, DMSO-d_6): δ 0.97 (s, 3H), 1.02 (s, 3H), 2.05 (d, 1H, J = 16.10 Hz), 2.20 (d, 1H, J = 16.10 Hz), 2.46 (m, 2H), 4.15 (s, 1H), 7.05 (s, 2H), 7.21 (m, 3H,), 7.29 (m, 2H).

2-Amino-4-(2,4-dichlorophenyl)-7,7-dimethyl-5-oxo-5,6,7,8-tetrahydro-4H-chromene-3-carbonitrile (**4i**).^{1}H NMR (400 MHz, DMSO-d_6): δ 1.05 (s, 3H), 1.17 (s, 3H), 2.17–2.25 (m, 2H), 2.54 (s, 2H), 4.55 (s, 1H), 5.91 (brs, 2H), 7.21–7.42 (m, 3H).

2-Amino-3-cyano-4-(4-cyanophenyl)-7,7-dimethyl-5-oxo-4H-5,6,7,8-tetrahydrobenzo[b]pyran (**4j**). ^{1}H NMR (400 MHz, DMSO-d_6): δ 0.93 (s, 3H), 1.02 (s, 3H), 2.10 (d, 1H, J = 16.00 Hz), 2.25 (d, 1H, J = 16.00 Hz), 2.51 (s, 2H), 4.29 (s, 1H), 7.14 (s, 2H), 7.35 (d, 2H, J = 8.10 Hz), 7.73 (d, 2H, J = 8.10 Hz).

6-Amino-4-(2-nitrophenyl)-5-cyano-2-methyl-4H-pyran-3-carboxylic acid ethyl ester (**4k**). ^{1}H NMR (500 MHz, DMSO-d_6): δ 0.91 (t, J = 7 Hz), 2.33 (s, 3H), 3.86–3.90 (q, J = 7 Hz, 2H), 5.01 (s, 1H), 7.07 (s, 2H), 7.40–7.87 (m, 4H).

6-Amino-4-(3-bromophenyl)-5-cyano-2-methyl-4H-pyran-3-carboxylic acid ethyl ester (**4l**). ^{1}H NMR (500 MHz, DMSO-d_6): δ 1.04 (t, J = 8 Hz, 3H), 2.32 (s, 3H), 3.91–4.04 (m, 2H), 4.32 (s, 1H), 6.99 (s, 2H), 7.15–7.44 (m, 4H).

2-Amino-4-(2-chlorophenyl)-7,7-dimethyl-5-oxo-5,6,7,8-tetrahydro-4H-chromene-3-carbonitrile (**4m**). ^{1}H NMR (400 MHz, DMSO-d_6): δ 0.95 (s, 3H), 1.00 (s, 3H), 2.07 (d, J = 16.1 Hz, 1H), 2.25 (d, J = 16.1 Hz, 1H), 2.60 (s, 2H), 4.38 (s, 1H), 7.02 (s, 2H), 7.13 (2d, J = 8.8 Hz, 2H), 7.41 (2d, J = 8.8 Hz, 2H).

2-Amino-4-(3-bromophenyl)-7,7-dimethyl-5-oxo-5,6,7,8-tetrahydro-4H-chromene-3-carbonitrile (**4n**). ^{1}H NMR (400 MHz,DMSO-d_6): δ 0.95 (s, 3H), 1.03 (s, 3H), 2.11 (d, J = 16.0 Hz, 1H), 2.25 (d, J = 16.0 Hz, 1H), 2.52 (s, 2H), 4.19 (s, 1H), 7.10 (s, 2H), 7.15 (d, J = 8.0 Hz, 1H), 7.26 (t, J = 8.0 Hz, 1H), 7.29 (s, 1H), 7.38 (d, J = 8.0 Hz, 1H).

2-Amino-4-(4-(dimethylamino)phenyl)-7,7-dimethyl-5-oxo-5,6,7,8-tetrahydro-4H-chromene-3-carbonitrile (**4o**). ^{1}H NMR (400 MHz, DMSO-d_6): δ 0.94 (s, 3H), 1.02 (s, 3H), 2.07 (d, J = 16.0 Hz, 1H), 2.23 (d, J = 16.0 Hz, 1H), 2.49 (s, 2H), 2.83 (s, 6H), 4.03 (s, 1H), 6.62 (d, J = 8.0 Hz, 2H), 6.89 (s, 2H), 6.92 (d, J = 8.0 Hz, 2H).

6-Amino-5-cyano-4-phenyl-2-methyl-4H-pyran-3-carboxylic acid ethyl ester (**4p**). ^{1}H NMR (500 MHz, DMSO-d_6): δ 1.08 (t, J = 7 Hz, 3H), 2.34 (s, 3H), 3.97–4.04 (m, 2H), 4.38 (s, 1H), 6.15 (s, 2H), 7.18–7.31 (m, 5H).

3 Results and discussion

Fe_3O_4@SiO_2-THDT nanocomposite was prepared by mixing THDT and Fe_3O_4@SiO_2. Firstly, THDT was synthesized from cyanuric chloride and hydrazine hydrate using nucleophilic reaction. Then, it was loaded on the external surface of Fe_3O_4@SiO_2-Cl using covalent bonding. Its structure was characterized by FTIR, thermogravimetric analysis (TGA), VSM, EDX, SEM, and XRD. For testing catalytic behavior, we utilize our synthesized catalyst in a model reaction named as pyran.

Figure 1, plots a–e, demonstrates the FTIR spectra of Fe_3O_4, Fe_3O_4@SiO_2, Fe_3O_4@SiO_2-Cl, and Fe_3O_4@SiO_2-THDT, respectively. Each preparation step of this complex can be traced using FTIR analysis. The indicator peak of magnetic Fe_3O_4 MNPs in Fig. 1(a) is related to Fe–O–Fe stretching vibration, which appears at around 586 cm^{-1}, and the peaks at around 1641 and 3455 cm^{-1} can be attributed to the HOH bending vibration of water and O–H stretching vibration. Figure 1(b) is ascribed to Fe_3O_4@-SiO_2. For Fe_3O_4@SiO_2, in Fig. 1(b), new peaks appear at 1087 cm^{-1}, which can be attributed to Si–O–Si asymmetric stretching vibration, and at 954 cm^{-1}, which belongs to Si–O–Si symmetric stretching. The formation of SiO_2 shell was confirmed at 810 cm^{-1} (in-plane bending) and 460 cm^{-1} (rocking mode) peaks. The weak bands validate the presence of attached alkyl groups at 2962 cm^{-1}, attributable to the C–H symmetric stretching mode of Fe_3O_4@-SiO_2@OSi $(CH_2)_3Cl$ (Fig. 1(c)). Upon adding THDT, the characteristic peak at around 1510 and 3313 cm^{-1} arises from the bending and stretching vibration of the primary amine group, and a sharp adsorption peak at 3319 cm^{-1} reveals a secondary amine group. A weak band at 1430 cm^{-1} corresponds to the C–C bond in the heterocyclic ring, and the existence of 1,3,5-triazole rings is confirmed through 802 cm^{-1} adsorption peak (Fig. 1(d)) [17,19]. Furthermore, it can be concluded that the nanostructure of THDT grafted-catalyst is well preserved after recycling, and it can be reused in model reaction more than 6 times without losing its significant catalytic activity (Fig. 1(e)). All of these bands confirm that functional groups were effectively attached to the synthesized novel MNPs.

Figure 2 shows the energy-dispersive EDX analysis of Fe_3O_4@SiO_2, Fe_3O_4@SiO_2-Cl, and Fe_3O_4@SiO_2-THDT nanocomposite. As illustrated in Fig. 2(a), the analysis proved the existence of nitrogen, oxygen, carbon, silicon, iron, and chlorine. Figure 2(b) demonstrates that core-shell structure is linked to Cl linker indicated by the presence of C and Cl elements. Figure 2(c) illustrates that N was detected. It is apparent that different elements including Fe, Si, O, and N were distributed inconsistently within the nanocomposite. Noteworthy, the amount of nitrogen is significant. Figure 2(d) confirmed that the content of the elements in the primary and recycled catalysts is very similar. To confirm the structure of the final product, XRD analysis was also performed. Elemental mapping of the Fe_3O_4@SiO_2-THDT nanocomposite reveal the presence of Fe, O, C, Si, and N (Fig. 2(e)).

3.1 Characterization of the prepared Fe_3O_4@SiO_2-THDT

We used SEM to study the morphology, structure, and size of the synthesized particles. As shown in Fig. 3(a), the morphology of Fe_3O_4@SiO_2-Cl magnetite exhibit particles that are dispersed with uniform and spherical morphology. Figure 3(b) illustrates the large porous THDT molecules attached to spherical Fe_3O_4@SiO_2-Cl nanocomposite. The principal reason for the porous

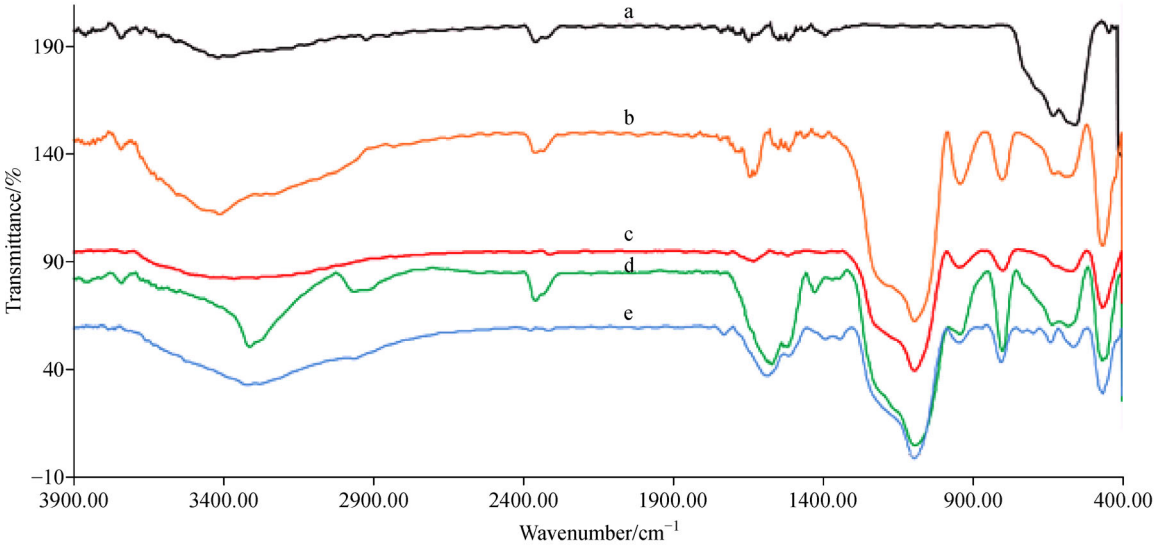

Fig. 1 Comparison of FTIR spectra for (a) Fe_3O_4, (b) Fe_3O_4@SiO_2, (c) Fe_3O_4@SiO_2-Cl, (d) Fe_3O_4@SiO_2-THDT and (e) recycled-Fe_3O_4@SiO_2-THDT.

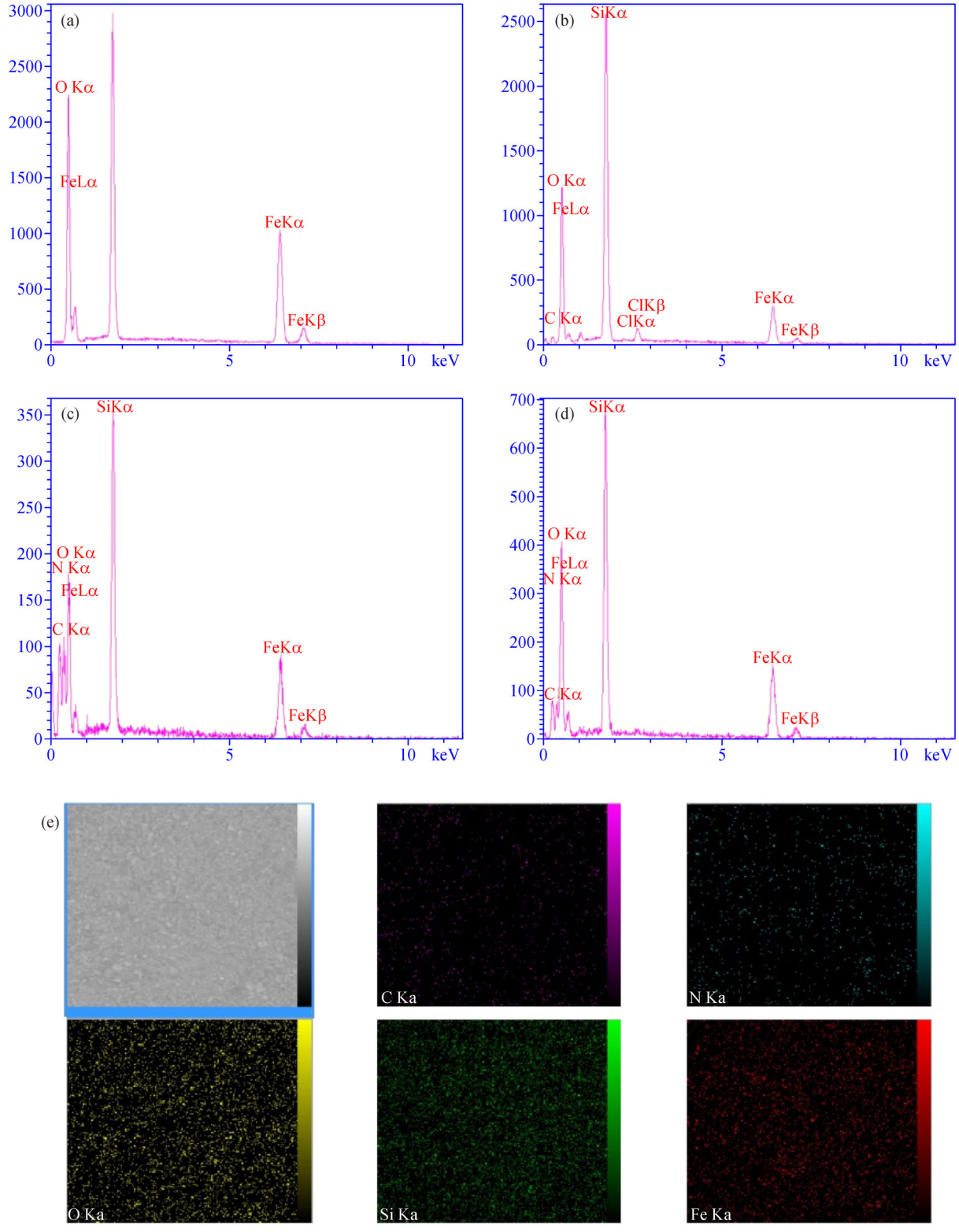

Fig. 2 EDX spectra of (a) $Fe_3O_4@SiO_2$, (b) $Fe_3O_4@SiO_2$-Cl, (c) $Fe_3O_4@SiO_2$-THDT and (d) recycled-Fe_3O_4-SiO_2@THDT; (e) elemental maps of Fe, O, Si, C, and N atoms (The scale bar is 1 μm. *y*-axis: number of counts (intensity), *x*-axis: energy (keV)).

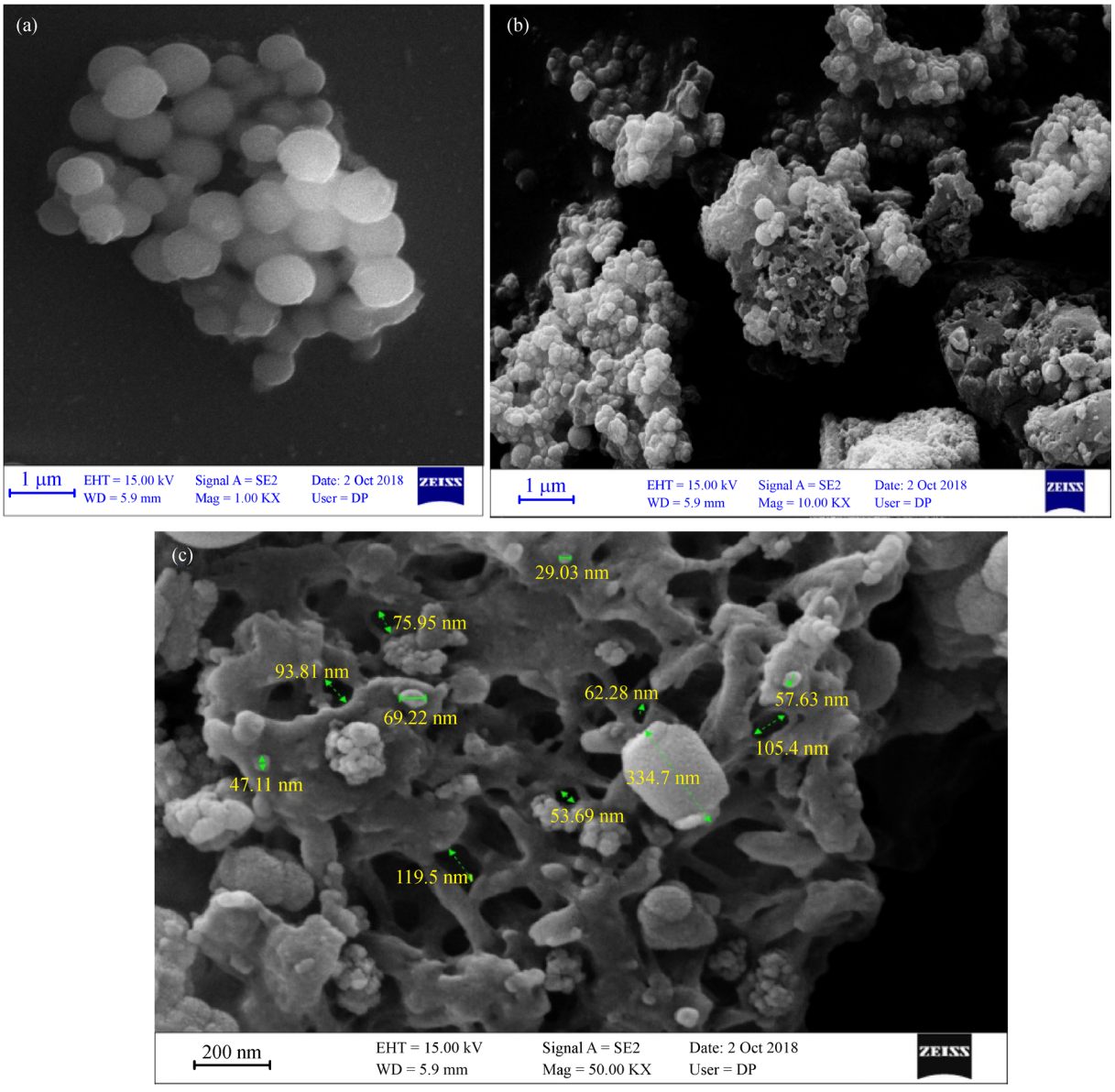

Fig. 3 SEM images of (a) Fe_3O_4@SiO_2-Cl microsphere, (b, c) Fe_3O_4@SiO_2-THDT.

structure of THDT is having a large number of amine groups. Figure 3(c) demonstrates the porous structure of THDT more effectively using a high resolution, magnified image.

VSM was used at room temperature to study the magnetic effect of the nanocomposite. The magnetization curves of Fe_3O_4, Fe_3O_4@SiO_2, and Fe_3O_4@SiO_2-THDT contain no hysteresis. Moreover, neither coercivity nor remanence was observed in their magnetization curves, confirming that all of them were superparamagnetic. Saturation magnetizations observed in the VSM curves were approximately 55 emu·g^{-1} for Fe_3O_4, 42 emu·g^{-1} for Fe_3O_4@SiO_2 and 23 emu·g^{-1} for the magnetite nanocatalyst. After recycling for more than six times, VSM analysis was performed and the magnetization was measured at 17.5 emu·g^{-1}. After the preparation of core-

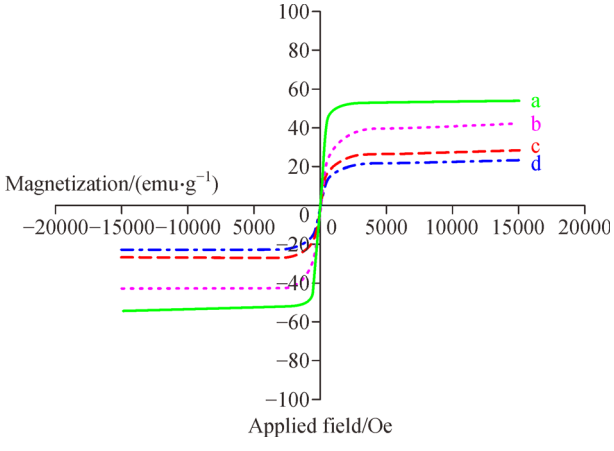

Fig. 4 VSM magnetization curves of (a) Fe_3O_4, (b) Fe_3O_4@SiO_2-Cl, (c) Fe_3O_4@SiO_2-THDT and (d) recycled-Fe_3O_4@SiO_2-THDT.

shell $Fe_3O_4@SiO_2$, the saturation magnetization decreased significantly. Nevertheless, as-prepared magnetite nanocatalyst has reasonable magnetic properties and could be effortlessly separated from the reaction mixture by an external magnet.

To investigate the thermal behavior of $Fe_3O_4@SiO_2$@THDT, magnetic nanocomposite TGA was performed in the temperature range of 20 °C –700 °C, under air atmosphere. The TGA curve is depicted in Fig. 5. The first weight reduction, from 50 °C to 150 °C, is related to the water absorption in the sample. The second weight reduction, appears from 280 °C to 305 °C, and coincides with the THDTs melting point, which is between 295 °C and 296 °C. The rest of the weight loss, 305 °C to 400 °C, occurs when THDT is decomposed. At 550 °C, the rest of the core-shell nanoparticles are decomposed. Therefore, Fig. 5 reveals a high amount of weight loss at 290 °C to 305 °C, where the THDT melting point belongs, confirming that THDT is loaded on the core-shell nanoparticles.

The X-ray diffraction pattern of the sample is presented in Fig. 6. The broad peak at 2θ between 19 and 24 indicates the presence of the amorphous SiO_2. Diffraction pattern showed characteristic peaks close to those of the Fe_3O_4 powder in the diffraction data peaks that has been reported: 30.44° (220), 35.81° (311),43.56° (400), 57.52° (511), 63.2° (400) (JCPDS19-629) [20].

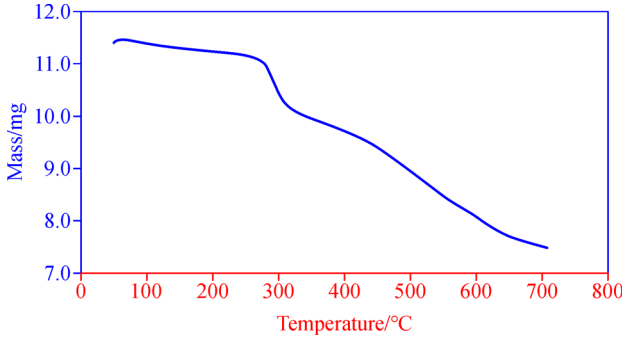

Fig. 5 TGA curve of $Fe_3O_4@SiO_2$-THDT.

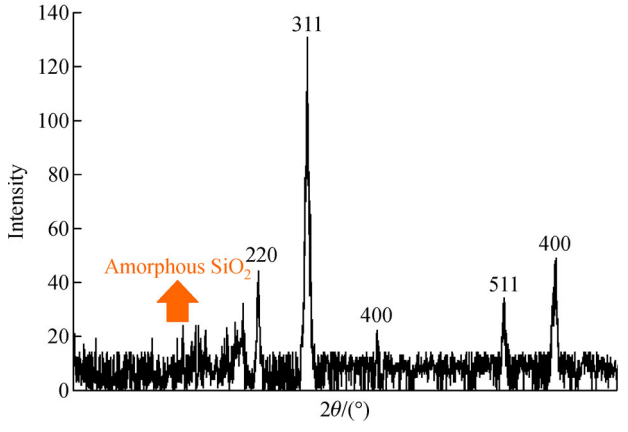

Fig. 6 The XRD pattern for $Fe_3O_4@SiO_2$-THDT.

Figure 7(a) shows the Raman spectra of Fe_3O_4. As observed in the figure, an intense peak at 699 cm^{-1} can be attributed to the stretch movements of Fe–O bond. There are other characteristic peaks at 320 and 560 cm^{-1}, confirming vibrational movements of Fe_3O_4. Low intensity peak at around 1400 cm^{-1} indicates impurities such as α-Fe_2O_3, γ-Fe_2O_3, and Fe–O–OH. Figure 7(b) shows Raman spectra of $Fe_3O_4@SiO_2$. In addition to the observed peaks of Fe_3O_4, which has positional shifts and intensity reduction, new peaks appear at around 220, 370 and 500 cm^{-1}, which are characteristic peaks for SiO_2. A peak at 370 cm^{-1} confirms the Fe–O–Si bond. Figure 7(c) shows Raman spectra of $Fe_3O_4@SiO_2@OSi(CH_2)_3Cl$. In addition to the previous peaks, a new peak appeared at around 1567 cm^{-1}, attributable to the C–Cl bond, and another at around 2920 cm^{-1}, attributable to CH_2. Also, C–C bond has a peak at around 300 cm^{-1}. Figure 7(d) shows the Raman spectra of as-synthesized catalyst. As the figure illustrates, in addition to the previous peaks, a new peak appeared at around 2000 cm^{-1}, confirming the C–N bond. Intense peaks before and after 1200 cm^{-1} confirms the formation of N–N and N–H bonds. Peaks around 790 and 1065 cm^{-1} are related to the trigonal ring. The 680 and 990 cm^{-1} peaks can be ascribed to carbon-amine and ring-nitrogen, respectively. Raman spectra of the recycled catalyst in Fig. 7(e), confirms that the structure is intact and that the catalyst can be reused several times [21].

3.2 Catalytic application of $Fe_3O_4@SiO_2$-THDT for the synthesis of tetrahydrobenzo[*b*]pyrans derivatives

We also studied the catalytic activity of the prepared nanocatalysts in the synthesis of tetrahydrobenzo[*b*]pyrans derivatives. To acquire optimal reaction conditions, we studied the condensation model reaction containing aryl aldehydes **1** (1.0 mmol), diketone **2** (1.0 mmol) and malononitrile **3** (1.0 mmol) in the vicinity of various catalytic amounts of $Fe_3O_4@SiO_2$-THDT at 75 °C in 3 mL of EtOH. Surprisingly, as little as 0.04 g of the synthesized catalyst was adequate to accelerate the reaction for obtaining high yields of tetrahydrobenzo[*b*]pyrans derivatives. The impact of solvent was also studied shown in Table 1. The results showed that the optimum solvent for the model reaction was EtOH, which had the highest efficiency among all solvents.

To test this catalyst in a variety of reactions, various aromatic aldehydes including electron donor derivatives were experimented, and different products were yielded under the optimal condition at 75 °C for 25 min. Thin-layer chromatography confirmed that after 25 min, the resulting product was obtained without any by-products, and the final product was highly pure. Finally, as provided in Scheme 2 and Table 2, all of the used aldehydes produced the desired product in a short reaction time and high yield.

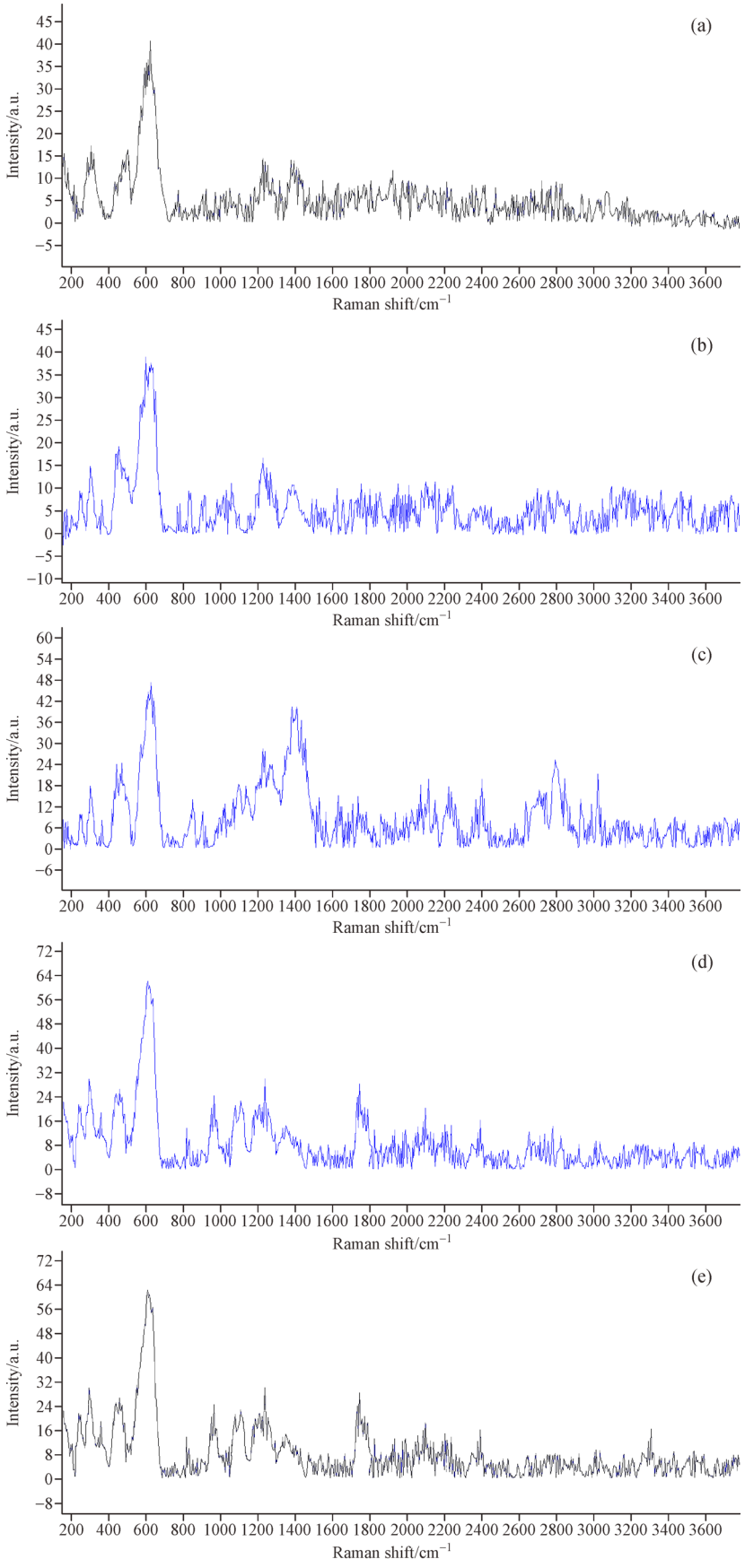

Fig. 7 Raman spectra of (a) Fe_3O_4, (b) Fe_3O_4@SiO_2, (c) Fe_3O_4@SiO_2-Cl, (d) Fe_3O_4@SiO_2-THDT and (e) recycled-Fe_3O_4@SiO_2-THDT.

Table 1 Reaction optimization of **4h** catalyzed by the Fe_3O_4@SiO_2-THDT

Entry	Solvent	Catalyst	Catalyst/g	Time/min	Yield/% [a)]
1	H_2O	–	–	60	Trace
2	H_2O	Fe_3O_4@SiO_2-THDT	0.04	60	21
3	EtOH	THDT	0.04	60	36
4	EtOH	Fe_3O_4	0.04	60	27
5	EtOH	Fe_3O_4@SiO_2	0.04	60	45
6	EtOH	Fe_3O_4@SiO_2-Cl	0.04	60	75
7	EtOH	Fe_3O_4@SiO_2-Cl	0.06	60	65
8	EtOH	Fe_3O_4@SiO_2-THDT	0.03	60	90
9	EtOH	Fe_3O_4@SiO_2-THDT	0.04	60	93
10	EtOH	Fe_3O_4@SiO_2-THDT	0.04	10	94[b)]
11	EtOH	Fe_3O_4@SiO_2-THDT	0.06	10	90

a) Isolated yield; b) The optimized conditions; benzaldehyde 1 (1.0 mmol), dimedone 2 (1.0 mmol) and malononitrile 3 (1.0 mmol) at 75 °C were used for the synthesis of **4h**.

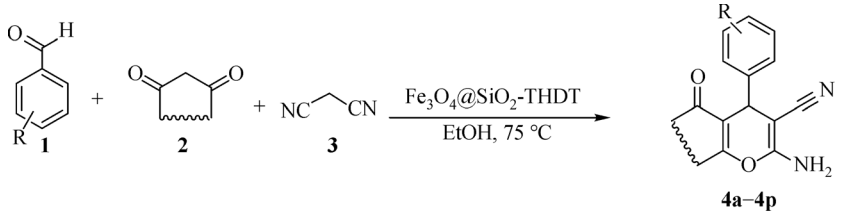

Scheme 2 Synthesis of tetrahydrobenzo[*b*]pyrans **4a**–**4p** using as-prepared catalyst Fe_3O_4@SiO_2-THDT at 75 °C.

Table 2 Reaction optimization of the synthesis of tetrahydrobenzo[*b*]pyrans **4a**–**4p** using as-prepared catalyst Fe_3O_4@SiO_2-THDT at 75 °C

Entry	Ar	1,3- Dicarbonyl compound	Product	Time/min	Yield/% [a)]	Mp/°C	
						Found	Reported
1	4-Chlorophenyl	Dimedone	**4a**	10	94	218–220	217–219 [22]
2	2-Methoxyphenyl	Dimedone	**4b**	16	84	203–205	200–201[22]
3	4-Hydroxyphenyl	Dimedone	**4c**	15	87	206–210	205–206 [24]
4	3-Hydroxyphenyl	Dimedone	**4d**	20	80	229-233	231–234 [22]
5	2-Methylphenyl	Dimedone	**4e**	25	82	207–210	205–207 [25]
6	3-Flourophenyl	Dimedone	**4f**	5	96	209–211	210–212 [23]
7	3-Nitrophenyl	Dimedone	**4g**	9	95	212–214	213-216 [22]
8	Phenyl	Dimedone	**4h**	10	93	231–233	229–231 [24]
9	2,4-Dichlorophenyl	Dimedone	**4i**	10	84	180–184	183–186 [23]
10	4-Cyanophenyl	Dimedone	**4j**	6	97	231–232	230–232 [22]
11	2-Nitrophenyl	Ethyl acetoacetate	**4k**	15	91	181–183	177–180 [26]
12	3-Bromophenyl	Ethyl acetoacetate	**4l**	12	86	169–171	166-167 [27]
13	2-Chlorophenyl	Dimedone	**4m**	15	80	290–292	289–291 [24]
14	3-Bromophenyl	Dimedone	**4n**	10	90	229–231	228–230 [23]
15	4-(Dimethylamino)phenyl	Dimedone	**4o**	7	93	214–216	212–213 [22]
16	Phenyl	Ethyl acetoacetate	**4p**	9	95	190–192	191–193 [25]

a) Isolated yield.

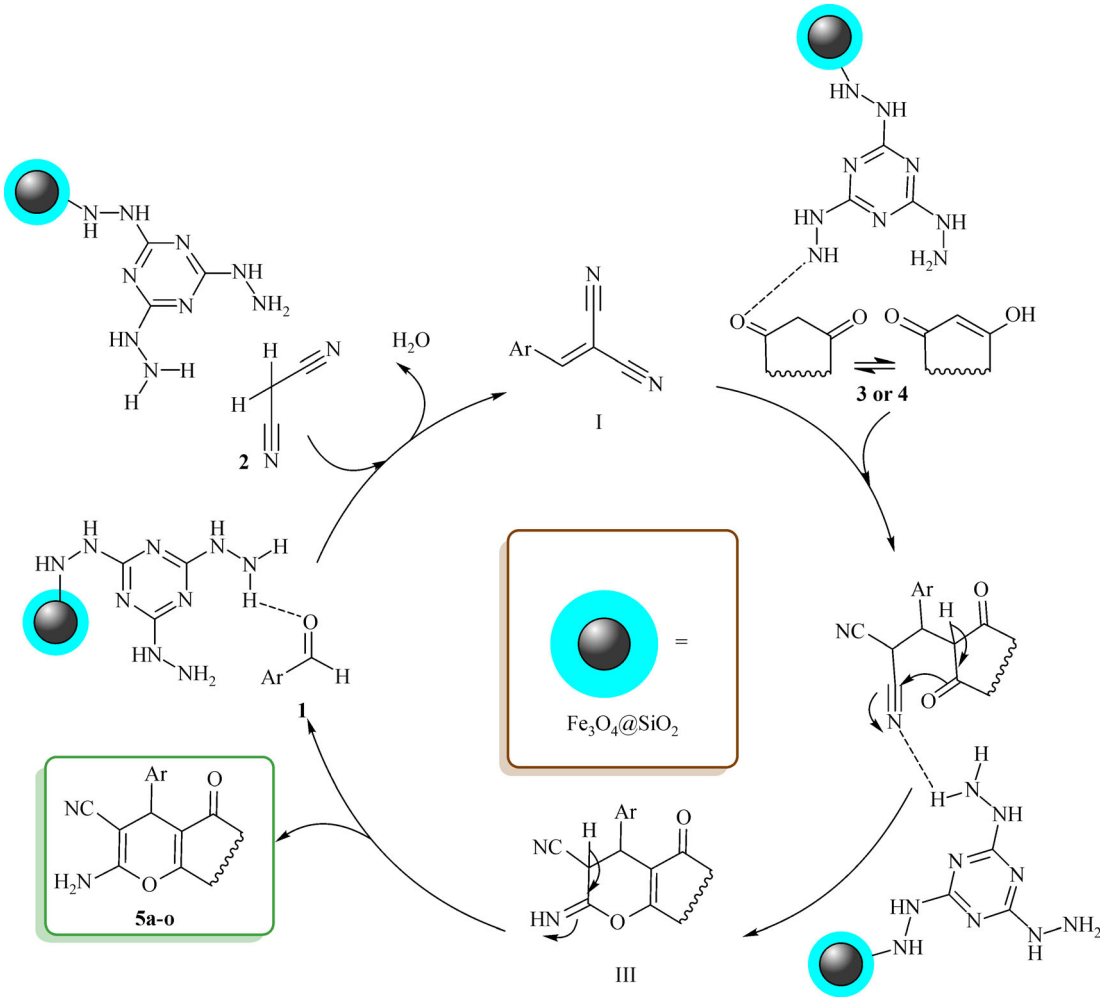

Scheme 3 Proposed mechanism for the synthesis of **4a**–**4p** using Fe_3O_4@SiO_2-THDT.

3.3 Mechanism evaluation

A suggested mechanism for the reaction is represented in Scheme 3. NH groups of THDT in Fe_3O_4@SiO_2-THDT nanocatalyst have increased the electrophilicity of aryl aldehydes as well as carbonyl carbon of C-H activated compounds. The reaction between an aromatic aryl aldehyde**,** and malononitrile **2** has formed Knoevenagel product **I**. The nanocatalyst has activated carbonyl diketone **3** or **4**. CH activated compound undergoes Michael addition with **I**, and the intermediate product **II** is obtained. The intermediate **III** endures intramolecular cyclization, followed by tautomerization, producing tetrahydrobenzo[*b*]pyrans derivatives **4a**–**4p**.

3.4 Recyclability of Fe_3O_4@SiO_2-THDT nanocatalyst

The synthesized catalyst is recyclable. It can be reused for at least six times without any significant change in its catalytic activity, which is highly helpful in commercial applications. In order to validate this claim, the catalyst was separated by an external magnet. After washing with ethanol and water and drying, it then was used in the reaction mixture. This procedure was repeated for at least six times. FTIR, EDX and VSM results confirmed that the catalyst activity has not been decreased significantly (Fig. 8).

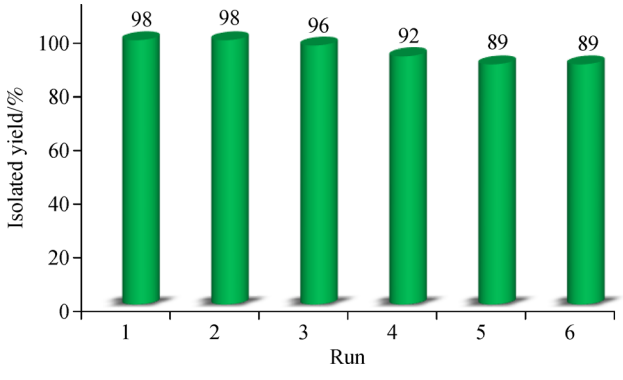

Fig. 8 Diagram of the recycled Fe_3O_4@SiO_2-THDT nanocatalyst in the synthesis of **4h**.

4 Conclusions

In this paper, we study the process for synthesizing Fe_3O_4@SiO_2-THDT nanocomposite by covalent bonding between THDT and silica-coated iron oxide nanoparticles. We first synthesized THDT from cyanuric chloride and hydrazine hydrate using nucleophilic reaction. We then attached THDT to the surface of Fe_3O_4@SiO_2-Cl using covalent bonding. The resulting product can decrease the reaction time of tetrahydrobenzo[*b*]pyrans preparation and its derivatives due to having several superficial NH groups. The formation of nanocomposite was confirmed by FTIR, EDX, TGA, VSM, SEM, and XRD. THDT has amine groups, and this can be confirmed by FTIR spectrum. Fe–O and Si–O bonding can also be confirmed using FTIR spectrum. The existence of nitrogen, carbon, oxygen, silicon, iron, and chlorine was verified using EDX analysis. XRD pattern showed peaks identical to standard cards of Fe_3O_4 MNPs and SiO_2. SEM images revealed the attachment of massive porous THDT molecules to spherical Fe_3O_4@SiO_2@OSi $(CH_2)_3$Cl nanocomposite. Based on the VSM curves, the synthesized nanoparticles saturation magnetization is about 20 emu · g^{-1}. TGA results proved that up to 295 °C, the nanocomposite was stable, without substantial mass loss. The as-synthesized catalyst can be easily separated by an external magnet, and can be recycled without loss of catalytic activity for at least 6 times. The production of this catalyst is eco-friendly, and using an environmentally-friendly and green process, it can be recycled in the synthesis of chemically crucial tetrahydrobenzo[*b*]pyrans. This novel catalyst can accelerate other chromene derivatives production and condensation reactions such as Knoevenagel.

Acknowledgements This work was partially supported by the research council of the Iran University of Science and Technology. We also would like to thank Maryam Niksefat, Ehsan Morshedloo and Peyman Hanifenejad for their help in graphic drawing.

References

1. Wu L, Mendoza-Garcia A, Li Q, Sun S. Organic phase syntheses of magnetic nanoparticles and their applications. Chemical Reviews, 2016, 116: 10473–10512
2. Polshettiwar V, Luque R, Fihri A, Zhu H, Bouhrara M, Basset J M. Magnetically recoverable nanocatalysts. Chemical Reviews, 2011, 111: 3036–3075
3. Maleki A, Rahimi J, Demchuk O M, Wilczewska A Z, Jasiński R. Green in water sonochemical synthesis of tetrazolopyrimidine derivatives by a novel core-shell magnetic nanostructure catalyst. Ultrasonics Sonochemistry, 2018, 43: 262–271
4. Wang D, Astruc D. Fast-growing field of magnetically recyclable nanocatalysts. Chemical Reviews, 2014, 114: 6949–6985
5. Hu Y, Zheng S, Zhang F. Fabrication of MIL-100(Fe)@SiO_2@-Fe_3O_4 core-shell microspheres as a magnetically recyclable solid acidic catalyst for the acetalization of benzaldehyde and glycol. Frontiers of Chemical Science and Engineering, 2016, 10(4): 534–541
6. Yuan E, Ren X, Wang L, Zhao W. A comparison of the catalytic hydrogenation of 2-amylanthraquinone and 2-ethylanthraquinone over a Pd/Al_2O_3 catalyst. Frontiers of Chemical Science and Engineering, 2017, 11(2): 177–184
7. Wu D, Xu F, Sun B, Fu R, He H, Matyjaszewski K. Design and preparation of porous polymers. Chemical Reviews, 2012, 112(7): 3959–4015
8. Bo L, Sun S. Microwave-assisted catalytic oxidation of gaseous toluene with a Cu-Mn-Ce/cordierite honeycomb catalyst. Frontiers of Chemical Science and Engineering, 2019, 13(2): 385–392
9. Mohapatra M, Anand S. Synthesis and applications of nano-structured iron oxides/hydroxides—a review. International Journal of Engineering Science and Technology, 2010, 2(8): 127–146
10. Maleki A, Azadegan S, Rahimi J. Gallic acid grafted to amine-functionalized magnetic nanoparticles as a proficient catalyst for environmentally friendly synthesis of α-aminonitriles. Applied Organometallic Chemistry, 2019, 33(5): e4810
11. Mohammadi A A, Asghariganjeh M R, Hadadzahmatkesh A. Synthesis of tetrahydrobenzo[*b*]pyran under catalysis of $NH_4Al(SO_4)_2 \cdot 12H_2O$ (Alum). Arabian Journal of Chemistry, 2017, 10: 2213–2216
12. Maleki A, Rahimi J, Hajizadeh Z, Niksefat M. Synthesis and characterization of an acidic nanostructure based on magnetic polyvinyl alcohol as an efficient heterogeneous nanocatalyst for the synthesis of α-aminonitriles. Journal of Organometallic Chemistry, 2019, 881: 58–65
13. Maleki A, Niksefat M, Rahimi J, Hajizadeh Z. Design and preparation of Fe_3O_4@PVA polymeric magnetic nanocomposite film and surface coating by sulfonic acid via *in situ* methods and evaluation of its catalytic performance in the synthesis of dihydropyrimidines. BMC Chemistry, 2019, 13(1): 19
14. Maleki A, Rahimi J. Synthesis of dihydroquinazolinone and octahydroquinazolinone and benzimidazoloquinazolinone derivatives catalyzed by an efficient magnetically recoverable GO-based nanocomposite. Journal of Porous Materials, 2018, 25(6): 1–8
15. Elhamifar D, Ramazani Z, Norouzi M, Mirbagheri R. Magnetic iron oxide/phenylsulfonic acid: a novel, efficient and recoverable nanocatalyst for green synthesis of tetrahydrobenzo[*b*]pyrans under ultrasonic conditions. Journal of Colloid and Interface Science, 2018, 511: 392–401
16. Maleki A, Hamidi N, Maleki S, Rahimi J. Surface modified SPIONs-Cr (VI) ions-immobilized organic-inorganic hybrid as a magnetically recyclable nanocatalyst for rapid synthesis of poly-hydroquinolines under solvent-free conditions at room temperature. Applied Organometallic Chemistry, 2017, 32(4): e4245
17. Dinari M, Hatami M. Novel *N*-riched crystalline covalent organic framework as a highly porous adsorbent for effective cadmium removal. Journal of Environmental Chemical Engineering, 2019, 7 (1): 102907
18. Taheri-Ledari R, Rahimi J, Maleki A. Method screening for conjugation of the small molecules onto the vinyl-coated Fe_3O_4/silica nanoparticles: highlighting the efficiency of ultrasonication. Materials Research Express, 2020, 7(1): 015067

19. Yaoting F, Gang L, Zifeng L, Hongwei H, Hairong M. Synthesis, structure and third-order nonlinear optical properties of 1,3,5-triazine-based Zn(II) three-dimensional supramolecule. Journal of Molecular Structure, 2004, 693(1-3): 217–224
20. Zhuang L, Zhang W, Zhao Y, Shen H, Lin H, Liang J. Preparation and characterization of Fe_3O_4 particles with novel nanosheets morphology and magnetochromatic property by a modified solvothermal method. Scientific Reports, 2015, 5(1): 9320
21. Huang H, Shende C, Sengupta A, Inscore F, Brouillette C, Smith W, Farquharson S. Surface-enhanced Raman spectra of melamine and other chemicals using a 1550 nm (retina-safe) laser. Journal of Raman Spectroscopy: JRS, 2012, 43(6): 701–705
22. Maleki A, Ghalavand R, Firouzi Haji R. Synthesis and characterization of the novel diamine-functionalized Fe_3O_4@SiO_2 nanocatalyst and its application for one-pot three-component synthesis of chromenes. Applied Organometallic Chemistry, 2018, 32(1): e3916
23. Khazaei A, Gholami F, Khakyzadeh V, Moosavi-Zare A R, Afsar J. Magnetic core-shell titanium dioxide nanoparticles as an efficient catalyst for domino Knoevenagel-Michael-cyclocondensation reaction of malononitrile, various aldehydes and dimedone. RSC Advances, 2015, 5(19): 14305–14310
24. Maleki A, Azadegan S. Preparation and characterization of silica-supported magnetic nanocatalyst and application in the synthesis of 2-amino-4-H-chromene-3-carbonitrile derivatives. Inorganic and Nano-Metal Chemistry, 2017, 47(6): 917–924
25. Zonouz A M, Okhravi S, Moghani D. Ammonium acetate as a catalyst and/or reactant in the reaction of dimedone, aromatic aldehyde, and malononitrile: synthesis of tetrahydrobenzo[*b*]pyrans and hexahydroquinolines. Monatshefte für Chemie-Chemical Monthly, 2016, 147(10): 1819–1824
26. Bodaghifard M A, Mobinikhaledi A, Asadbegi S. Bis(4-pyridylamino) triazine-stabilized magnetite nanoparticles: preparation, characterization and application as a retrievable catalyst for the green synthesis of 4H-pyran, 4H-thiopyran and 1,4-dihydropyridine derivatives. Applied Organometallic Chemistry, 2017, 31(2): e3557
27. Niknam K, Borazjani N, Rashidian R, Jamali A. Silica-bonded *N*-propylpiperazine sodium *n*-propionate as recyclable catalyst for synthesis of 4H-pyran derivatives. Chinese Journal of Catalysis, 2013, 34(12): 2245–2254